Spring 5-2013

Developing Methods to Measure Small Attenuation Coefficients Using Short Distance Radiation Detection

Erica F. Bloor
University of Southern Mississippi

The University of Southern Mississippi

Developing Methods to Measure Small Attenuation Coefficients Using Short Distance Radiation Detection

by

Erica Bloor

A Thesis
Submitted to the Honors College of
The University of Southern Mississippi
in Partial Fulfillment
of the Requirements for the Degree of
Bachelor of Science
in the Department of Physics

April 2013

Approved by

_____

Chris Winstead

Professor of Physics

_____

Khin Maung, Chair

Department of Physics and Astronomy

_____

David R. Davies, Dean

Honors College

Abstract

Accurate radiation measurements are very important for a variety of health, security, and industrial applications. The work described in this thesis is based upon developing a correction for the response of a sodium iodide (NaI) gamma-ray detector that is accurate enough to be used for determination of small mass-attenuation coefficients, such as for air, with short distance measurements. The goal is to find and apply appropriate corrections for the raw data provided by the NaI detector to enable the measurement of the gamma-ray mass-attenuation coefficients of air for detection distances of less than 1 meter. If measurements of the mass-attenuation coefficient of air produce values comparable to those provided by the National Institute of Standards and Technology, the results and experimental and analysis processes have the potential to help researchers correct radiation detection data from long range measurements.

Key Terms: Gamma-ray measurements, sodium iodide detector, mass attenuation coefficient, detector efficiency correction

Contents

Chapter 1 Introduction

With so many sources of harmful radiation, being able to detect radiation from far away is becoming more and more relevant. The interaction of radiation in our atmosphere from high energy cosmic rays or byproducts of nuclear weapons development can change the composition of our atmosphere and ultimately our environment and us. In order to correctly determine how much radiation was originally emitted from a radiation source, the mass-attenuation coefficients of the materials between the source and the detector must be known. Being able to determine the mass-attenuation coefficient of such materials will give the researcher a more accurate analysis of the actual strength of a source of radiation by allowing a correction for attenuation to be calculated. More accurate values for even small mass-attenuation coefficients will help with long range detection for purposes such as national security and academic research.

The purpose of this research is to determine if we can apply a geometric correction for the detection response of sodium iodide (NaI) detectors accurately enough to measure small mass-attenuation coefficients, such as for air, using short distance measurements. By finding and applying appropriate corrections for the raw data provided by the NaI detector, we should be able to determine the mass-attenuation coefficient of air using detection distances less than 2 meters. If we are in fact able to measure the mass-attenuation coefficient of air – similar to values provided by the National Institute of Standards and Technology – our results and experimental and

analysis processes will help researchers correct radiation detection data for air attenuation.

Even though accepted values for small mass-attenuation coefficients such as that of air are widely used in radiation calculations, these values may not take into consideration important variables regarding the material through which the radiation is transmitting. Air, for instance, changes with altitude and humidity. The mass-attenuation coefficient for air depends on these variables, and our goal is to see if we can measure specific mass-attenuation coefficients of air through an experimental process which can be easily employed in almost any environment.

Chapter 2 Background

2.1 Radiation

Radiation is a term applied to the whole electromagnetic spectrum, from low energy radio waves to visible light to high energy gamma rays. The energy of such radiation is given by the relationship between wavelength and the speed of light:

$$E = \frac{hc}{\lambda}$$

where h is Planck's constant ($6.626x10^{-34}$ Joules second), c is the speed of light in a vacuum ($2.998x10^{8}$ meters per second), and λ is the wavelength. This inversely proportional relationship between the energy and wavelength tells us that as the wavelength becomes smaller, the energy per radiated photon becomes greater.

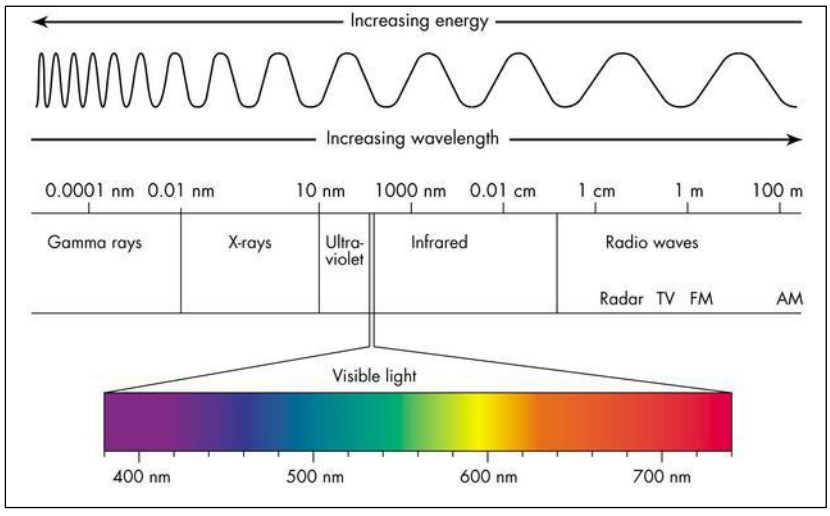

Figure 2.1 The Electromagnetic Spectrum. Visual representation of the spectrum of radiation showing relationship between wavelength and energy. <http://www.cyberphysics.co.uk/topics/light/emspect.htm>

Radiation can be classified as non-ionizing or ionizing [1]. Non-ionizing radiation has a low frequency which can interact with atoms but not ionize them [2]. Non-ionizing radiation sources are shown with their energies, frequencies, and sources in Table 2.1 below [3].

Energy	**Frequency**	**Type of radiation**	**Sources**
0 eV– 1.38×10^{-20} eV	0 Hz–300 kHz	Low frequency to extremely low frequency electromagnetic radiation (LF–ELF)	Electrical fields of devices, conventional electrical network, video monitors, sections of AM radio
1.38×10^{-18} eV –1.38×10^{-23} eV	3 kHz–300 MHz	Radio frequencies (RF)	Sections of AM radio, FM radio, medical short-wave, nuclear magnetic resonance (NMR)
1.38×10^{-23} eV –1.38×10^{-26} eV	300 MHz–300 GHz	Microwave (MW)	Domestic microwave devices, mobile telephones, microwave for medical physical therapy, radar and other microwave communications
1.38×10^{-26} eV – 1.59 eV	300 GHz–780 nm	Infrared (IR)	Solar light, heat and laser therapy devices
1.59 eV – 3.10 eV	780 nm–400 nm	Visible light	Solar light, phototherapy, laser
3.10 eV – 12.41 eV	400 nm–280 nm	Ultraviolet (UV)	Solar light, fluorescent tubes, food/air sterilization, radiotherapy, etc.
	Hz: Hertz (kHz: kilohertz = 10^3 Hz; MHz: Megahertz s = 10^6 Hz; GHz: Gigahertz = 10^9 Hz). Ultraviolet (UV) within the range 280–185 nm is considered as ionizing radiation.		

Table 2.1 Energies, frequencies and sources of non-ionizing radiation.
Comparison of different types of non-ionizing radiation. [3].
<http://www.sciencedirect.com/science/article/pii/S0048969710003104>

Ionizing radiation (IR) is the most energetic form that can severely affect atoms [2]. Ionization occurs when an electron is completely stripped from an atom, implying the energy provided from the radiation is enough to overcome the binding energy of the electron in its shell. For living organisms, this can destroy the DNA within the cell by single-strand breaks, oxidative damage, and double-strand breaks, which are the most threatening to biological cells [4]. Forms of IR are gamma rays, x-rays, and some high energy UV rays, which can cause these mutations in DNA and ultimately cancer [1]. However, IR is also used in radiotherapy to treat cancer by attacking the cancer cells. It is a form of indirect IR which involves a two step process: the photons incident on a material release electrons which then deposit energy in the substance through orbital electron interactions [5]. The Compton scattering effect is a common mechanism of the ionization of an atom at x-ray and gamma ray energies (see Figure 2.2).

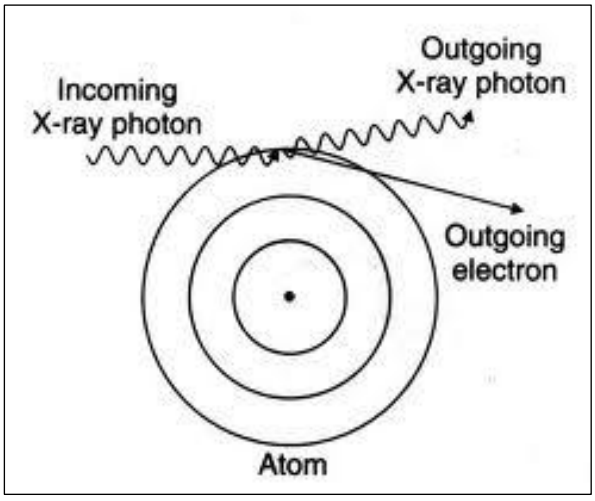

Figure 2.2 Compton Scattering Effect.
An incoming photon interacts with an electron from an orbital of an atom, ionizing the atom (removing an electron which takes energy) and the leftover energy is carried off by a second photon. [6]
<http://wiki.uiowa.edu/display/881886/CT+Dictionary>

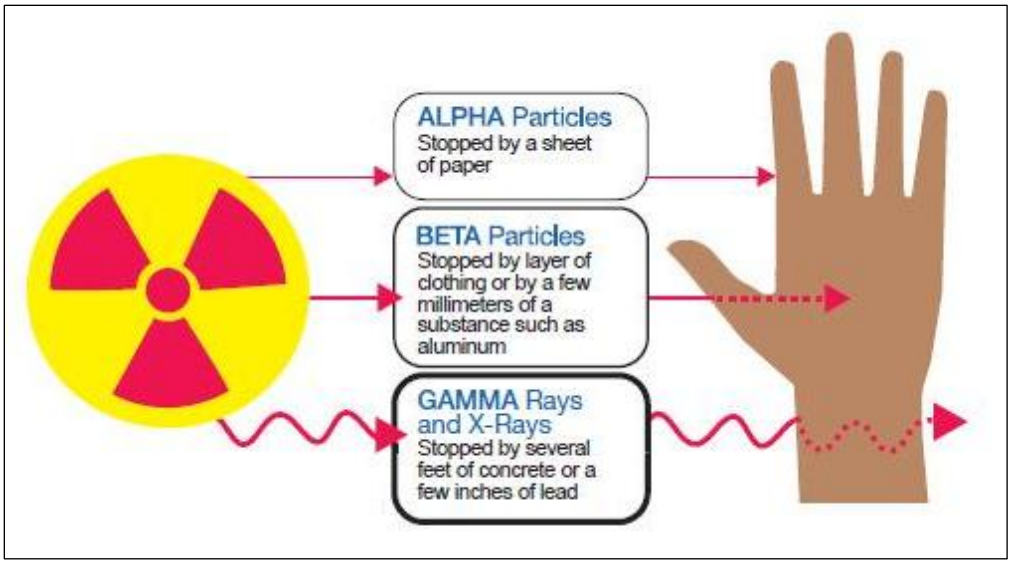

Figure 2.3 Penetration of Alpha, Beta, and Gamma Radiation.
The depth of penetration through human tissue by the three types of ionizing radiation. [2] < http://www.epa.gov/radiation/docs/402-f-06-061.pdf>

IR can be divided into 3 groups: alpha radiation, beta radiation, and gamma radiation. Figure 2.3, provided by the Environmental Protection Agency, shows the depth of penetration of alpha, beta, and gamma rays on human tissue. The penetration depth increase from one type of radiation to the next is shown by the thicknesses of the lines representing each type. Alpha and beta radiation are charged particles emitted from a source. Alpha radiation is a heavier particle – a Helium nucleus – that can only travel short distances and is not able to penetrate human skin or clothing. Beta radiation is a light particle – an electron – that can penetrate human skin to a level that it may be harmful depending on the duration of exposure. Gamma ray radiation was mentioned earlier because a gamma ray is a photon and thus has no weight or mass, but is very penetrating: several feet of concrete or a few inches of lead would be needed in order to stop gamma rays [2]. The amount of radiation absorbed or transmitted depends on the

radiation energy and the thickness and attenuation coefficient of the materials it is being induced upon.

Gamma radiation is created when a parent nucleus decays and its daughter nucleus still has excess energy. This energy is lost when the daughter nucleus emits a pulse of electromagnetic radiation – a gamma ray [7]. For Cesium-137, the atom undergoes beta decay prior to the emission of a gamma ray. Cesium 137 emits a gamma ray in 93.5% of all decays as it first undergoes beta decay into Barium-137m (662 keV) then gamma decay into Barium 137. A diagram of this process is shown in Figure 2.4. 6.5% of Cs-137 decays are purely beta decay, resulting in no gamma emission. What will be detected is technically the Barium-137 atom gamma-ray with 662 keV, but we still consider this Cs-137 detection.

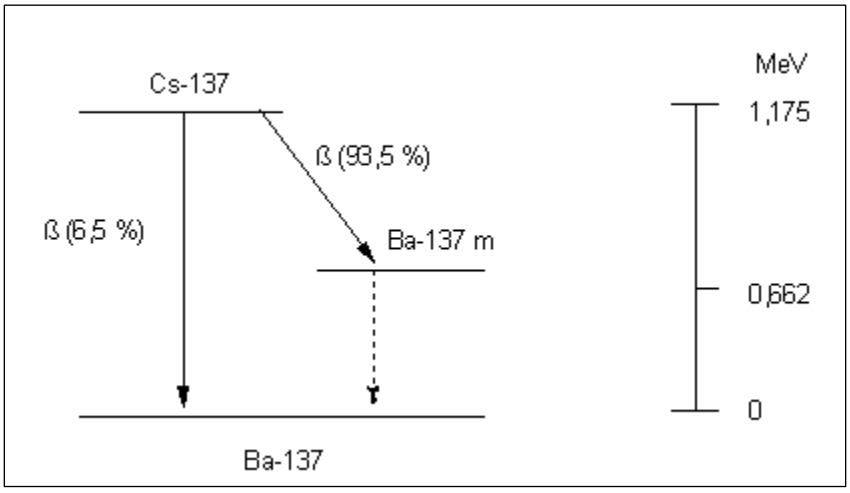

Figure 2.4 Cesium-137 Decay.

2.2 Mass Attenuation Coefficients

The ability of a material to transmit or attenuate radiation is quantified by its mass attenuation coefficient, μ/ρ. Mass attenuation coefficients characterize how much intensity of incident radiation is lost as the radiation transits a material. The units for mass attenuation coefficient are length squared per mass ($cm^2 g^{-1}$). We can obtain μ/ρ from the equation for a beam of photons with an incident intensity penetrating a material:

$$\frac{I}{I_o} = \exp[-(\mu)x]$$

I_o: incident intensity

I: emerging intensity

μ: attenuation coefficient where $\mu = \left(\frac{\mu}{\rho}\right)\rho$

ρ: material density

x: mass thickness of material

The attenuation coefficient – a function of the photon's energy – can now be written as [8]:

$$\mu = -x^{-1} \ln\left(\frac{I}{I_o}\right)$$

This value is a basic quantity used to find the penetration and energy deposition of photons in materials which is essential in many branches of physics, including dosimetry, interferometry, and radiography. Although the mass attenuation coefficient is defined here in terms of the effect of a material on a beam of photons, it can also be used with appropriate corrections for other geometries.

Our values obtained from calculations will be compared to values provided by NIST [8]. The attenuation coefficients provided in the NIST databases are not listings of other experimental measurements, but are values calculated using more fundamental quantities such as cross-sections for the photoelectric effect, Compton scattering, Rayleigh scattering, and pair production. In turn, these cross-sections have been measured in a variety of experiments performed over the last several decades, with results being refined over time until a general consensus has been achieved. For photon interactions, such as for gamma-rays, these various cross-sections and the resulting attenuation coefficients are collected in the XCOM database. XCOM is the source of the attenuation coefficients provided in the NIST X-Ray attenuation database.

2.3 Scintillation Detector

A scintillator is a material that produces photons when interacting with ionizing radiation [9]. The first scintillator was used by Rutherford in 1910 for alpha-scattering experiments. A scintillation system consists of four basic parts: the scintillant (gas, liquid or solid material), a photo-multiplier, a power supply, and an "amplifier-analyzer-scaler system" as shown in Figure 2.5 [10].

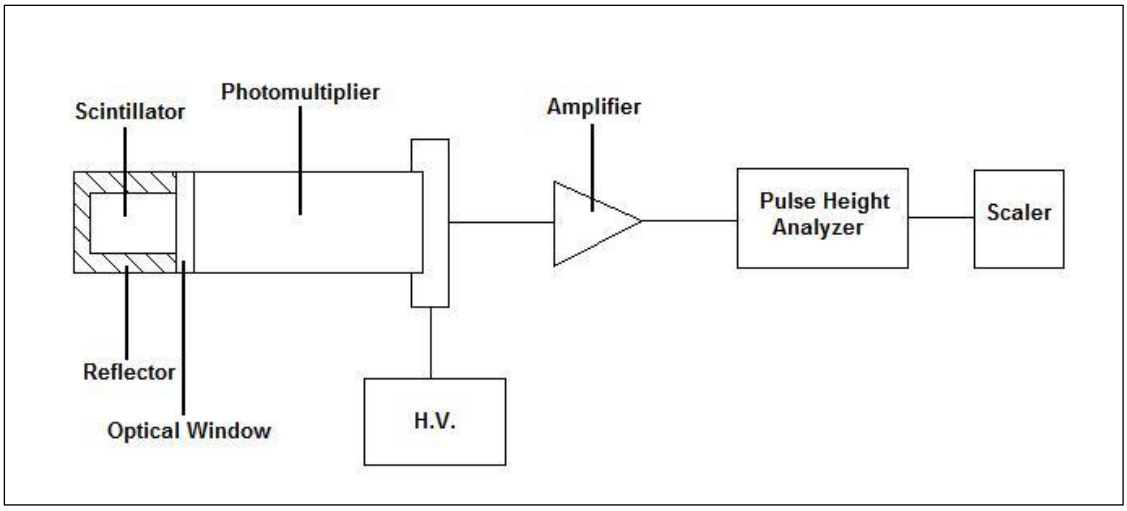

Figure 2.5 Scintillator System Diagram

The scintillator first absorbs incident radiation energy and produces photons with frequencies in the visible part of the electromagnetic spectrum. The intensity of the flash of light produced within the scintillator is proportional to the energy of the absorbed radiation. The scintillator photons strike the photocathode of a photomultiplier tube within the detector which produces an electronic pulse for some fraction of the photons depending upon the quantum efficiency of the detector. A count rate is recorded from these electronic pulses.

There are two types of scintillants: inorganic and organic. Organic scintillants have a non-linear relationship between the pulse height and energy, whereas inorganic scintillants yield a linearly proportional relationship between pulse height and a wide range of energy [10]. For our experiment using gamma rays, the inorganic scintillant will produce a linear relationship because the scintillant will receive energy from the electrons produced by the incident gamma rays. Gamma rays interact in the scintillator by the photoelectric effect, the Compton Effect, or pair production [10]. The electrons produced

in any of these processes excite the scintillant, which then produces the photons. This is how we can conclude that pulse height is proportional to the energy of the electron and ultimately the energy of the gamma ray.

For the experiment described later, an ORTEC NaI detector will be used. The ORTEC detector counts the number of photons produced from interactions within the NaI crystal by gamma rays from our Cs-137 source and plots the counts in Maestro, a program included with the ORTEC detector (see Figure 2.6). This program produces a graph of counts versus energy which indicates the intensity of the incident radiation at a particular distance between the source and the detector. The pulse height distribution for any gamma ray source gives us three distinct points: a backscattered peak, a Compton edge, and a photo peak which accounts for the incident radiation source. The chart also shows background noise of low energy radiation of the surrounding environment. Below are charts of the total counts of Cs-137 and Cobalt-57 for 2 minutes at 10 centimeters as examples of counting using the Maestro program. Note the difference in peak energy between Cs-137 (661 KeV) and Co-57 (122 KeV) in the graphs.

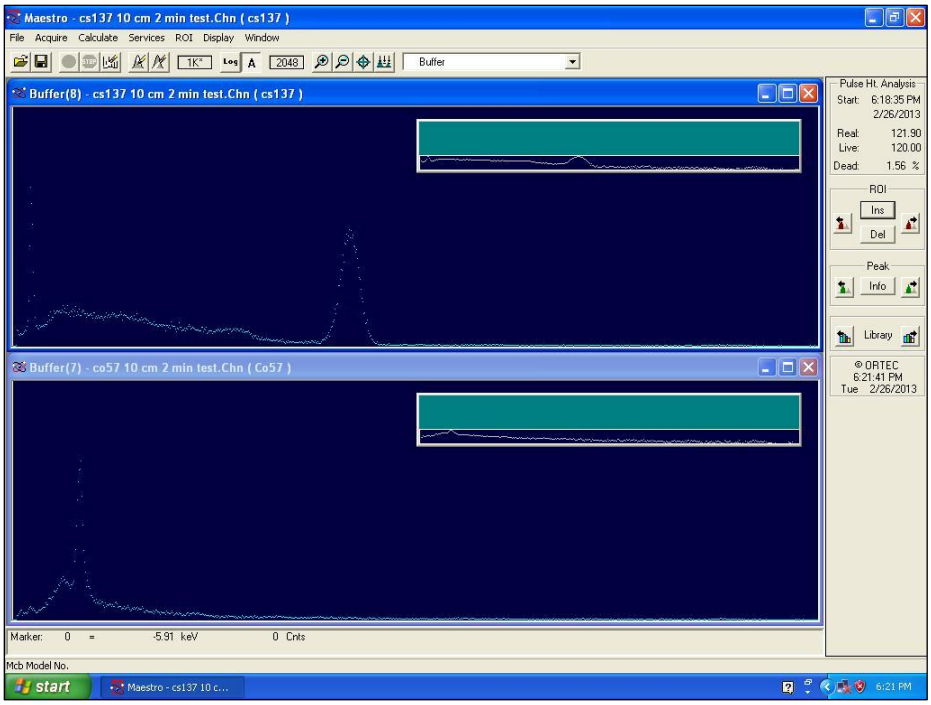

Figure 2.6 Example Graphs of Source Peaks.
The graph of Cs-137 is the top graph, and Co-57 is the bottom graph. These are plots of energy (x-axis) versus counts (y-axis).

The backscattering peak found near the lower energy end of the Cs-137 graph is a result of the primary photons that were scattered by nearby shielding material now being absorbed by the crystal. The Compton edge is created when an atomic electron undergoes the Compton Effect instead of the photoelectric effect. The scintillation photons as a result of that process correspond to the energy given up to the Compton electron which gives us a "Compton continuum" from zero to the Compton edge [11]. The photo peak represents the number of pulses produced by the photoelectrons produced by photo-ionization, corresponding to the radiation source energy [10].

The most commonly used scintillator with a high efficiency is the sodium iodide crystal. It is an inorganic scintillant which allows for a greater light output. The NaI scintillant is a large clear crystal that must be sealed in an airtight can because it is highly

sensitive to humidity, and is used mainly for gamma ray and charged particle detection [10, 11]. According to Wang, NaI has a "high attenuation coefficient for the interaction of gamma rays," and the best resolution for a 662 keV gamma ray from a Cs-137 source for a 3 inches diameter by 3 inches long NaI crystal is about 7% [12].

2.4 Detector Efficiency

Without knowledge of the detector efficiency, it is impossible to quantify the emission rate of a source. A significant aspect in radiation detection is the efficiency of the detector. The following calculation is used to determine the effect of distance on detector efficiency, following a derivation by Tsoulfanidis, but also incorporates new modifications made to include the attenuation coefficient for air [9]. Most calculations for the detector efficiency completely neglect any corrections for attenuation due to air because the attenuation coefficient is small, but our calculations incorporate this factor for a more precise result. Figure 2.7 shows the quantities that will be used to make the efficiency calculations.

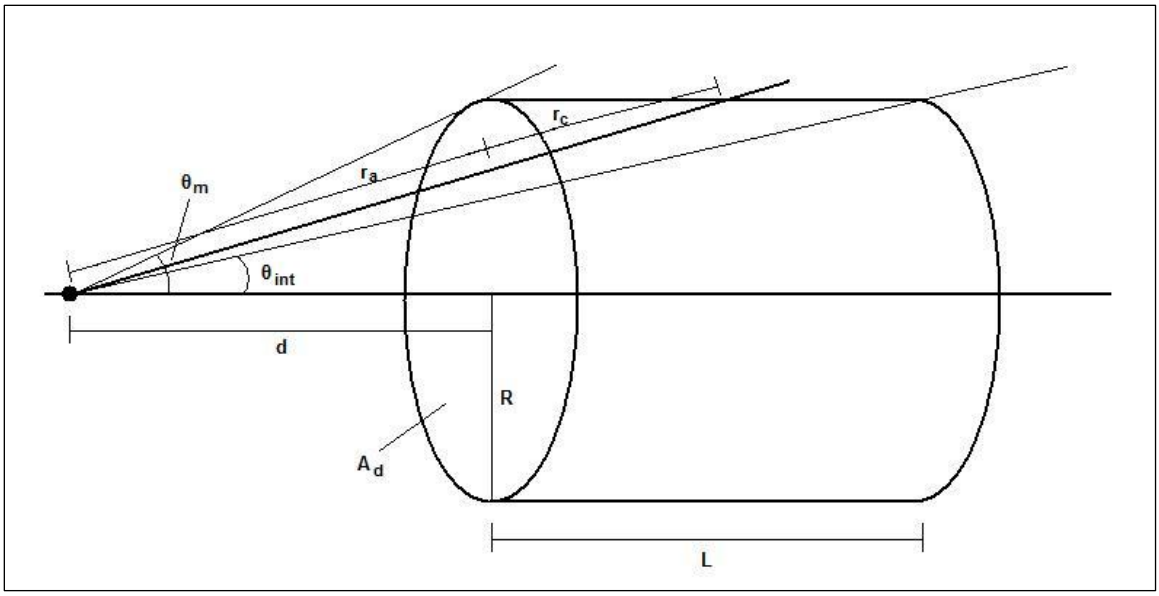

Figure 2.7 Volume Correction for Scintillator

S: emission rate of gamma rays

d: distance from the source to the face of the detector

A_d: surface area of the face of the detector

θ_m: maximum angle to hit detector

θ_{int}: angle to the rear corner of the crystal

r_a: distance traveled in air from the source to the detector (function of θ)

r_c: distance traveled in crystal (function of θ)

μ_a: attenuation coefficient of air

μ_c: attenuation coefficient of crystal

The efficiency incorporates the following probabilities:

- the probability that a gamma ray from the source is not attenuated by air along the path length (r_a): $e^{-\mu_a r_a}$

- the probability that the gamma ray is emitted between the angles θ and $\theta + d\theta$: $\frac{1}{2}\sin\theta\, d\theta$
- the probability that the gamma ray interacts within the crystal to produce a pulse of light (i.e. that it does not transmit through the crystal): $1 - e^{-\mu_c r_c}$.

The probability for detection of a gamma ray emitted at an angle between θ and θ+dθ is proportional to

$$\frac{1}{2}(1 - e^{-\mu_c r_c})e^{-\mu_a r_a} sin\theta d\theta.$$

In order to find the efficiency for detection, we integrated the probability over angles from zero to θ_m. Our efficiency equation now looks like:

$$\varepsilon = \int_0^{\theta_{int}} \frac{1}{2}(1 - e^{-\mu_c r_c})e^{-\mu_a r_a} sin\theta d\theta + \int_{\theta_{int}}^{\theta_m} \frac{1}{2}(1 - e^{-\mu_c r_c})e^{-\mu_a r_a} sin\theta d\theta$$

Note that r_c changes depending on whether θ is less or greater than θ_{int}:

- For $0 < \theta < \theta_{int}$, $r_c = \frac{L}{cos\theta}$.
- For $\theta_{int} < \theta < \theta_{max}$, $r_c = \frac{R - dtan\theta}{sin\theta}$.

2.5 Inverse Square Law

Just as the intensity of light falls off proportional to the square of the distance between a point light source and observer, radiation also follows the inverse square law.

Radiation spreads out as it travels away from the source and therefore becomes weaker as it spans a larger area [13]. The inverse square law has the following equation where d is the distance from the source to the detector:

$$Intensity \propto \frac{1}{d^2} = d^{-2}$$

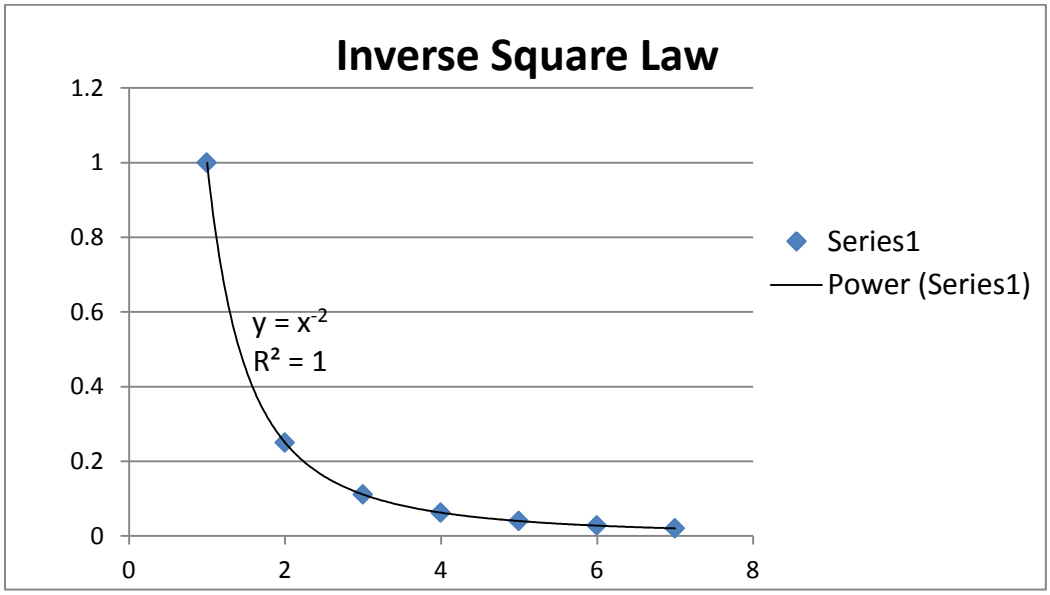

Figure 2.8 Graph of the Inverse Square Law for 7 Data Points

Chapter 3 Materials

3.1 Detector and Program

For our experiment, we used an ORTEC 3x3 Integral NaI and 296 Tube Assembly. This detector included a 3x3 Sodium Iodide cylinder crystal, ScintiPack Model 296 photomultiplier base with preamplifier, and high voltage power supply. A picture of this assembly is shown in Figure 3.1 below. Included with the scintillator detector assembly is a digiDART-LF digital portable MCA (multichannel analyzer), seen on the left in Figure 3.1, used for gamma-ray spectroscopy. This digiDART-LF is intended for use with the NaI detector. The detector, seen on the right in Figure 3.1, is connected to the portable MCA which is then connected to the computer,.

Figure 3.1 ORTEC Detector and digiDART-LF System

3.2 Radiation Source

We used a small source of Cesium 137 to collect data. Cesium 137 has a half life of about 30 years, which was ideal for our experiment so that we would not need to worry about the source decaying quickly. Our source of Cs 137 is shown below.

Figure 3.2 Cesium-137 Radiation Source

3.3 Structural Equipment

In order to create the desired setup for this experiment, we needed enough space to move the source at least 1 meter away from the detector. Below is the list of supplies we used to create our experimental setup:

- Optics bench
    - Used for support of the radioactive source and easy measurement of the distance from the source to the detector
- Average size cardboard box

    - Used as support for detector and lifted the detector away from dense objects such as the lab table
- Wooden dowel, support, and binder clip
    - The support for the wooden dowel allowed the dowel to be moved along the optics bench easily. The radiation source was placed on the wooden dowel with the binder clip at the same height as the face of the detector. A wooden dowel was chosen as a low density mount for the radiation source to minimize scattering of the gamma rays.
- Computer
    - On which programs were used to collect and analyze data.

Chapter 4 Experimental Procedure

Below is a basic outline of the experimental process:

- Experimental Setup: Placement of optics bench, source support, and detector support; connection of equipment to computer program.
- Data Acquisition: Open Maestro program and collect data for source at varying distances from the detector and save data.
- Data Analysis: Open collected data in Cambio program; manipulate graphs and calibrate to obtain total counts as area under the curve.

4.1 Equipment Setup

The first objective was to create a setup that lifted the scintillation detector far away from dense objects such as a lab table or other machinery in the lab. On the lab table, a board was secured on top of two projections about 1 foot high. Then an average-size cardboard box was set on top of the board and the scintillation detector was set on top of that to reduce clutter of dense materials near the source and detector as well as background radiation noise. Then an optics bench was placed perpendicular to the box but parallel to the detector. On the bench, a wooden dowel which holds the radiation source was anchored. The radiation source was secured onto the wooden dowel with a medium-size binder clip at a vertical distance that aligned with the face of the detector. The basic setup is shown in Figure 4.1.

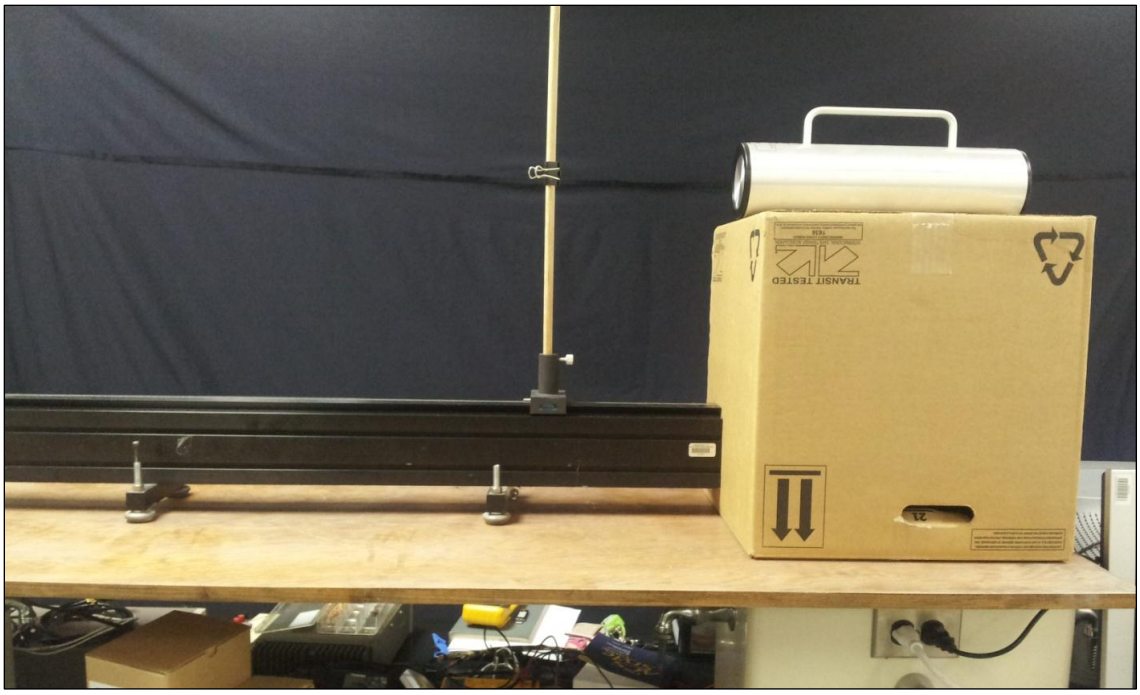

Figure 4.1 Experimental Setup for Radiation Detection

4.2 Data Acquisition

Once this setup was complete, detection trials were taken with the Cs-137 source. Using gloves, the Cs-137 source was secured into the binder clip, making sure the height of the source on the pole matched the face of the detector. Data was taken from 7 points along the optics bench in increments of 15 cm: 10 cm, 25 cm, 40 cm, 55 cm, 70 cm, 85 cm, and 100 cm. These several points provided data spanning varying distances within a meter.

To start a data run using the NaI detector, the Maestro software settings must be entered. One very important entry is the live-time. The live-time is the actual time the detector is ready to count. The detector is "dead" for a very short amount of time during

each detection while it records a photon count. So the live-time is the time the detector is available to count photons, whereas the real time is the total time it takes for a data run (which may be several seconds longer than live-time). The software tracks the live-time of the detector so that each run counts for the same amount of live time, regardless of the count rate (which strongly impacts the time the detector is unavailable). In Figure 4.2, the live-time preset is set to 20 minutes. A 40 minute or longer preset for the live-time allowed the observation of the Cs-137 photopeak even at 100 cm. Maestro also includes a tab labeled "About" where notes can be recorded about the data run – like which radiation source was being used.

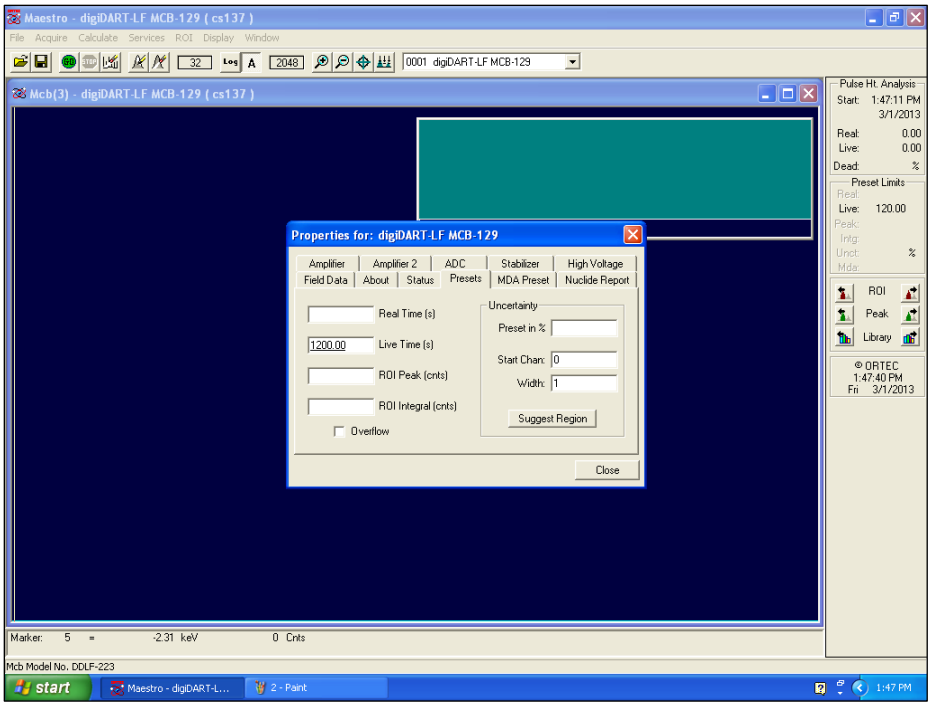

Figure 4.2 Live-Time Preset

Once the Maestro program was prepared, the radiation source was positioned at one of the 15 cm increment distances. A notch on the right side of the radiation source support was used to read the position of the support on the optics bench. When the

middle of the source was at a distance x, the far right side of the notch was estimated to be at $x + 4.9$ cm. After the support had been moved to the appropriate distance and the alignment of the source and detector was checked, detection and data collection began. Seen on the screen were counts at different energies as well as the real and live times running on the side bar.

After each data run was completed, the spectrum was saved, and the support was moved to begin taking data again at a different position. The total time to take data for 7 points and for background noise (data run without source) was about 5 to 6 hours.

Once all data runs were saved, the Cambio software – developed at Sandia National Laboratories – was then used to find the area under the photo peak curve. Cambio was used rather than Maestro because it allowed for greater ease when analyzing the graphs of the count rates. The area under the photo peak was actually the total number of counts between two specific energies. Upon opening the Cambio program, there were two windows: one for viewing and manipulating the graphs, and one for viewing and collecting data for the graph. The background noise data run was opened first and made to be the reference spectrum as shown in Figure 4.3. The background spectrum was obtained without the radiation source present in order to be subtracted from the source data. This removed contributions from background radiation from the data analysis. The background subtraction was performed using the live-time scaling option in Cambio (as shown in Figure 4.4) to ensure that the subtraction was performed properly even if the background and source spectra live-times were different.

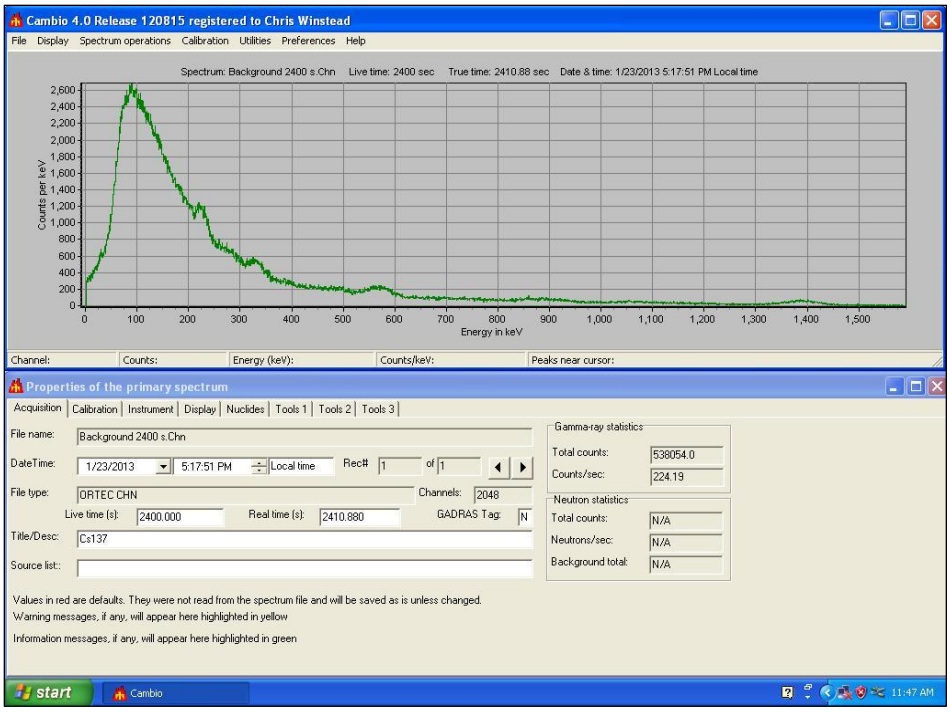

Figure 4.3 Background Spectra in Cambio

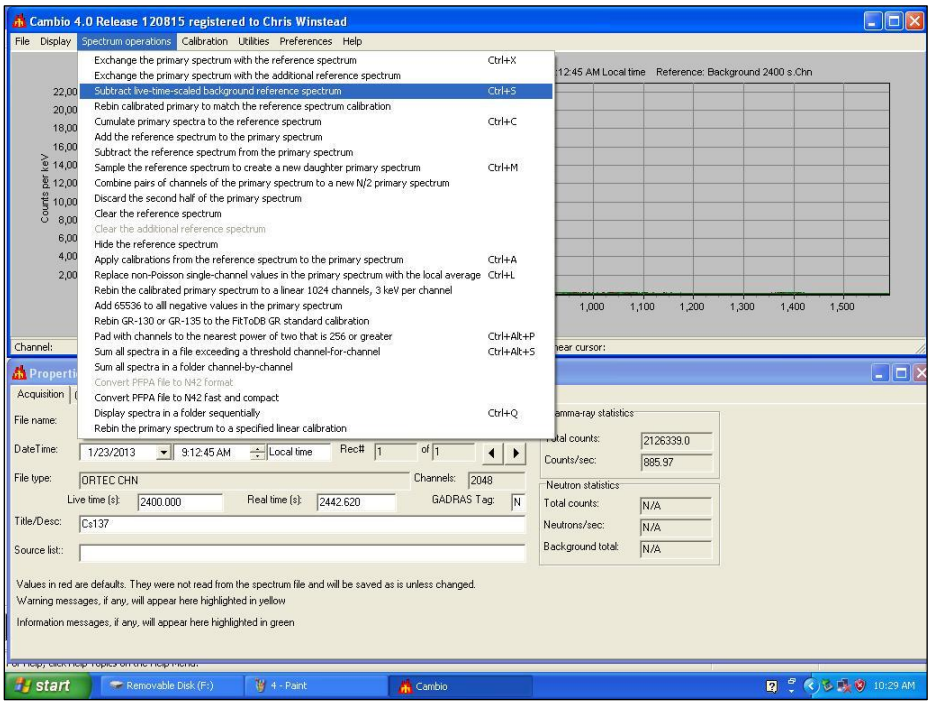

Figure 4.4 Subtraction of Live-Time Data

The next series of steps provided the area under the curve and curve fit data. The frame for the horizontal channel scale was set to 775-930, which from experience was known to center the window on the Cs-137 photopeak. This scale set the window for the Cambio program to count the total number of counts in that window of the data. After the frame was applied, the "Acquisition" tab showed the gamma-ray statistics such as the total counts as seen in Figure 4.5. However, the graph needed to be calibrated in order to obtain correct total counts. An auto-calibration function within the Cambio software could be used for energy calibration of the data by assigning the peak as a Cs-137 gamma peak, and returning the display frame to the prior window gave a repeatable number for the total counts (Figures 4.6 and 4.7). The total counts were used in calculations of the attenuation coefficient of air.

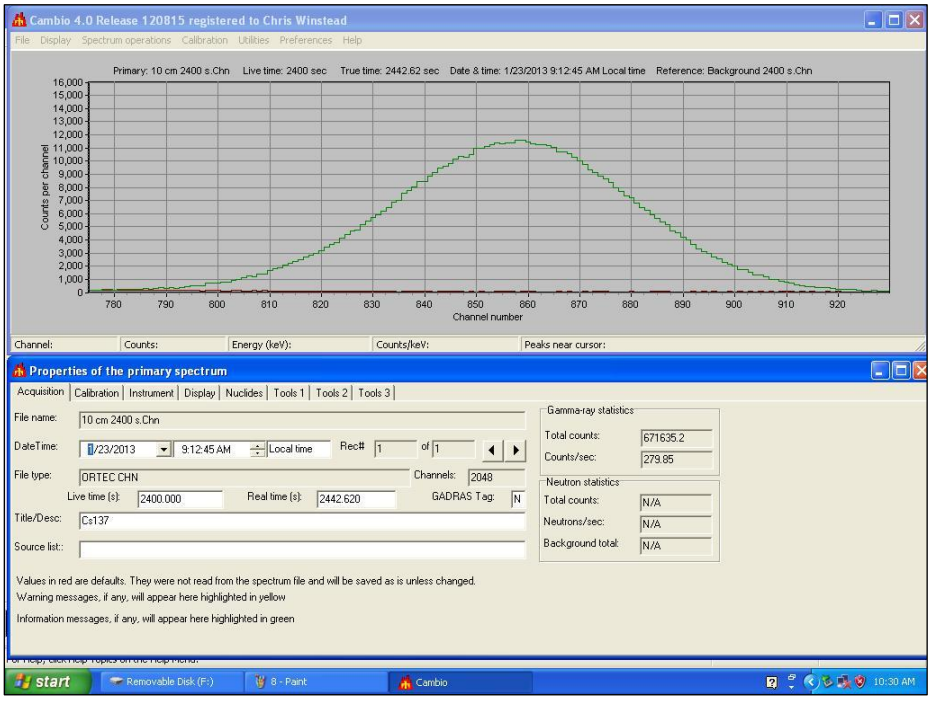

Figure 4.5 Total Counts

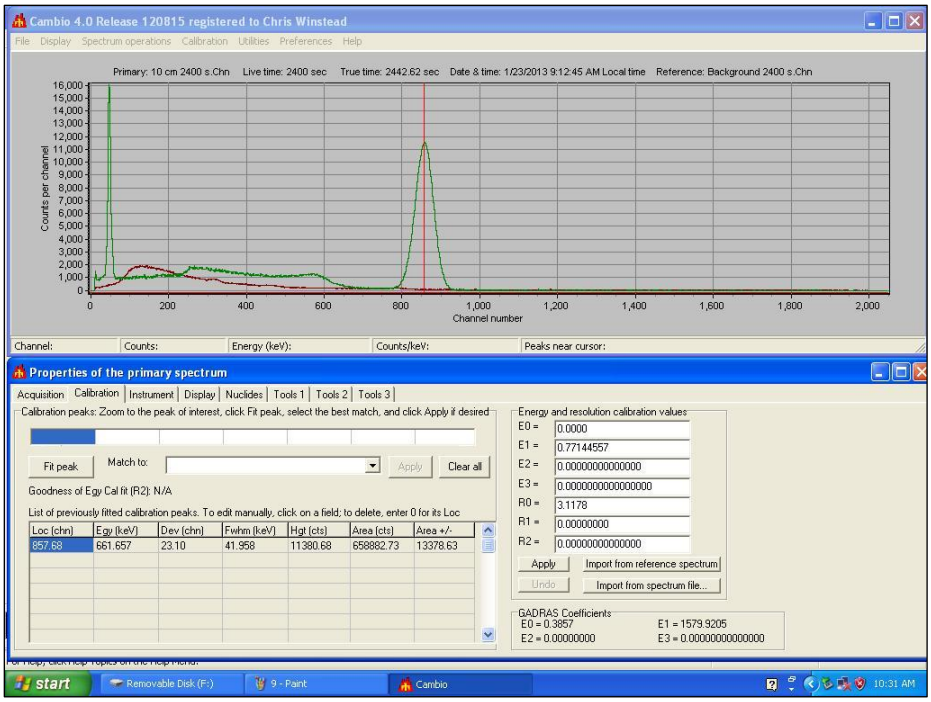

Figure 4.6 Calibration and Curve Fit

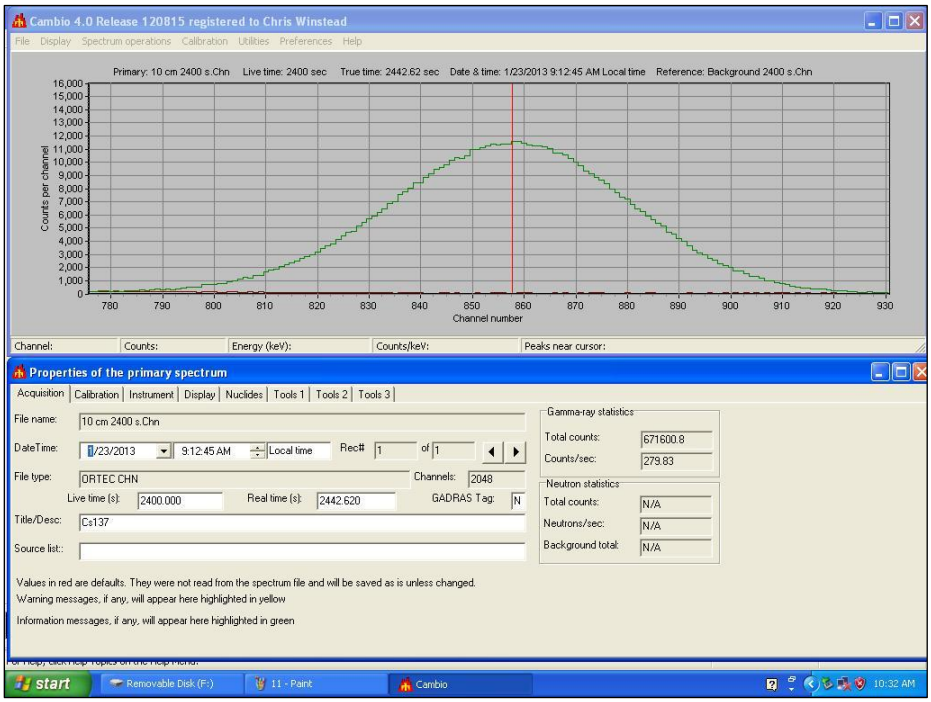

Figure 4.7 Correct Total Counts

4.3 Data Analysis Procedure

Two sets of data were obtained for the total counts generated by the source at each of the chosen distances. The first step for data analysis is to combine all data into a spreadsheet, using Microsoft Excel for example. The average of the two data sets, the standard deviation, and the percent difference were found using Microsoft Excel to check for significant differences between the two data sets. A plot of the recorded data was generally in line with the expectations for a graph of total counts versus distance, the curve showed that the count rate was high near the detector, then dropped off quickly for short distances and more slowly as the distance was increased (as shown in Figure 4.8).

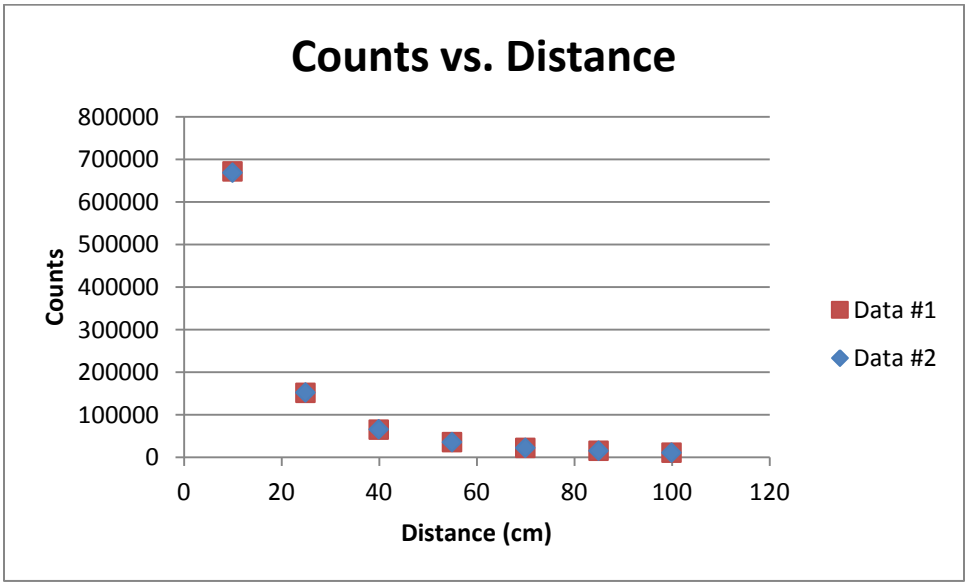

Figure 4.8 Total Counts versus Distance Plot

In order to correct this data for the different detector efficiencies appropriate for different distances, a correction for the scintillator response as explained in "Detector Efficiency" above was needed. Trapezoidal integration, for this data analysis, was used to best approximate the area under the curve using many trapezoids with a width $\Delta\theta$ and

heights that meet the curve. A FORTRAN program that asked for an input of number of trapezoids to estimate the area under the curve and the attenuation coefficient of air was created to help with this correction. (Although the ultimate goal is to find the attenuation coefficient of air, the process of inputting varying values for the attenuation coefficient of air into the program will help find a value that best fits the data.) After these values were entered, the program presented the total efficiency at each of the chosen distances. Below is the program created to find the efficiency; it printed the results into a separate file and on the screen.

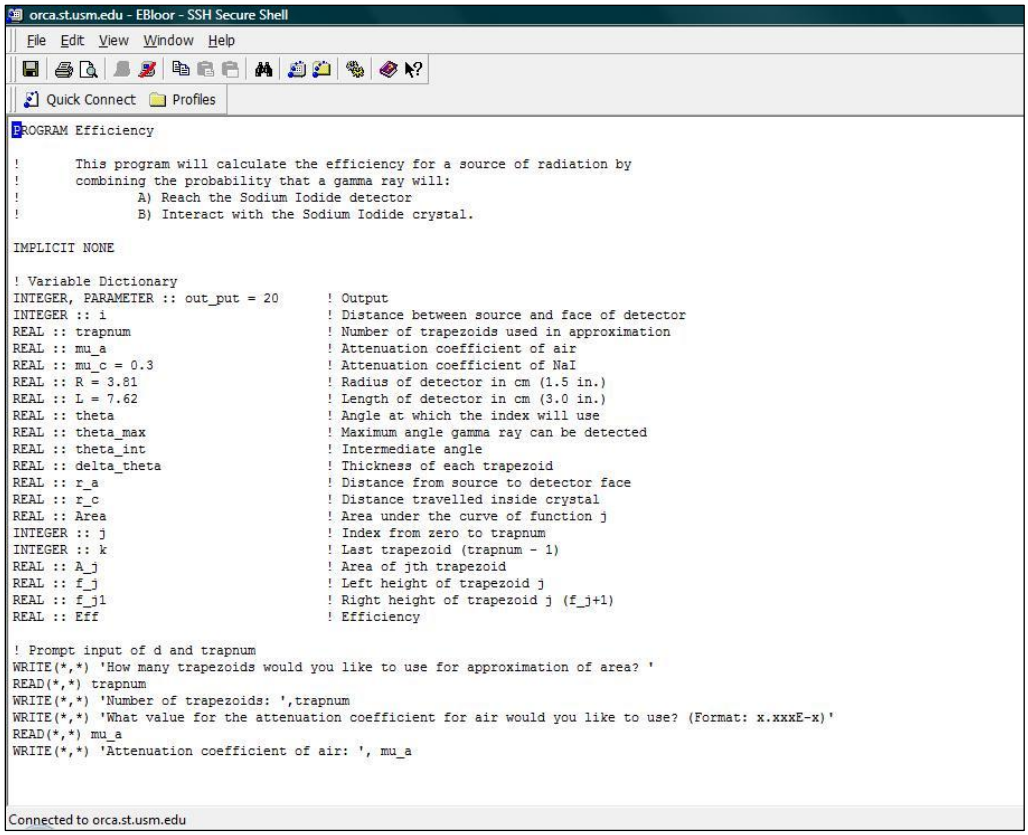

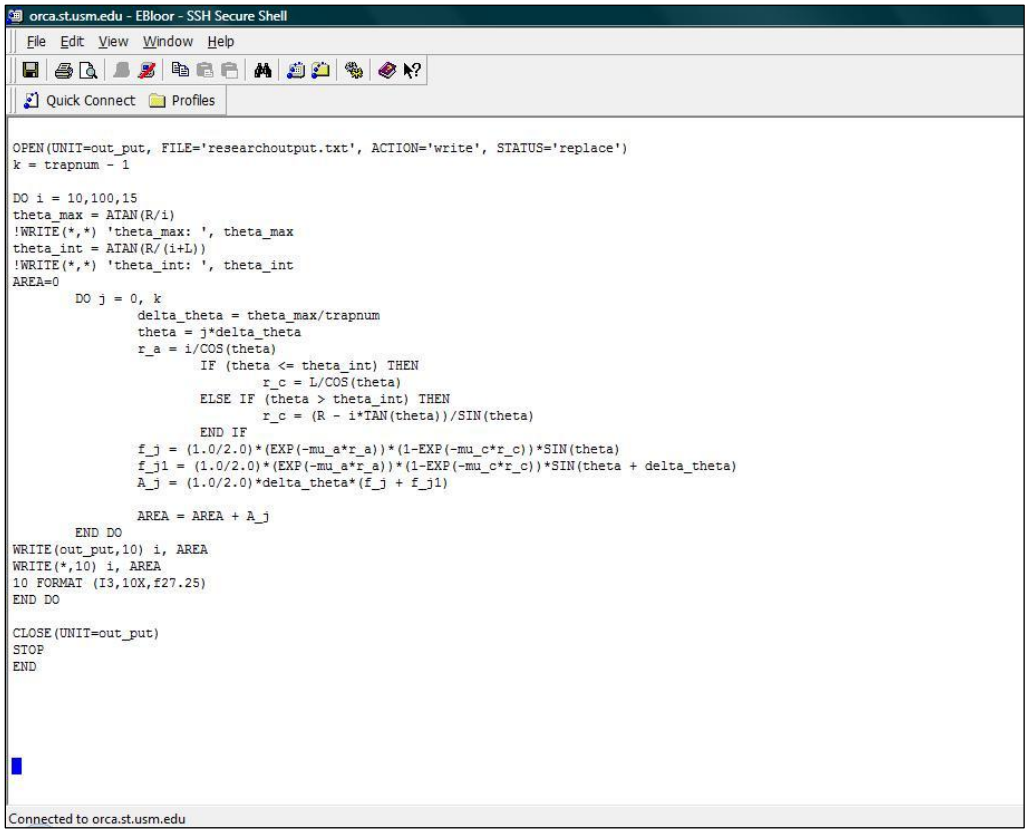

Figure 4.9 Efficiency Program

Once values for total efficiency were obtained for each distance, the average total count values were divided by their respective efficiency values to produce a value proportional to the total emission count of the Cs 137 source. For example, if the average total count rate for 25 cm was 150,000 counts and the total efficiency value for 25 cm was 0.0040 (or 0.40%), then the total emission count for Cs 137 is proportional to $\frac{150{,}000\ counts}{0.0040} = 37{,}500{,}000\ counts$. Once this process of dividing the average total counts by the efficiency was completed, values for the total emission were produced and then plotted. The values for the total emission are expected to be approximately the same value since the total emission count of Cs 137 is constant at any distance. The plot of the values for total emission count should have produced a straight horizontal line if the values were the same, but the line produced with the data was not straight, so varying values for the attenuation coefficient of air were used to try to straighten out the line. The value for the attenuation coefficient of air that gives the straightest line is expected to be close to the value given by NIST.

Chapter 5 Data and Analysis

5.1 Detection of Cesium 137

The first objective for the experimental process was to collect data for the detection of our Cs 137 source. Two data runs for a Cs 137 source were collected at the below distances, for which the detector ran for a live-time of 40 minutes. The data below show the count rate for each data run determined using the Cambio program. Also included is the average of the counts produced in the two data runs, giving the value used in the calculations. The standard deviation and percent difference are also included to allow the difference in the data between the two runs to be seen.

Cesium 137						
	Data #1	Data #2				
CM	AREA	AREA	AVERAGE	Standard Deviation	Percent Difference	
10	671639.1	668540.8	670089.95	2190.82894	0.00326946	0.33%
25	151979.3	152770.2	152374.75	559.250753	0.00367023	0.37%
40	65390.7	65667.2	65528.95	195.515025	0.00298364	0.30%
55	35632.1	36044.0	35838.05	291.257283	0.00812704	0.81%
70	22149.1	22686.4	22417.75	379.928474	0.01694766	1.69%
85	15536.7	15424.2	15480.45	79.5495129	0.00513871	0.51%
100	11108.3	11463.0	11285.65	250.810775	0.02222387	2.22%

Table 5.1 Counts for Varying Distances

The results confirmed the expectation that the count rate between distances will drop drastically similarly to the inverse square law. This can be seen in the graph of the average total count versus the distance below. If there were no air attenuation of the gamma rays and the Cs-137 source was actually a point source and there was no

difference in detector efficiency with distance, the count rate would fall at $1/r^2$ according to the inverse square law. In this graph, the power is -1.792, a significant difference from -2.

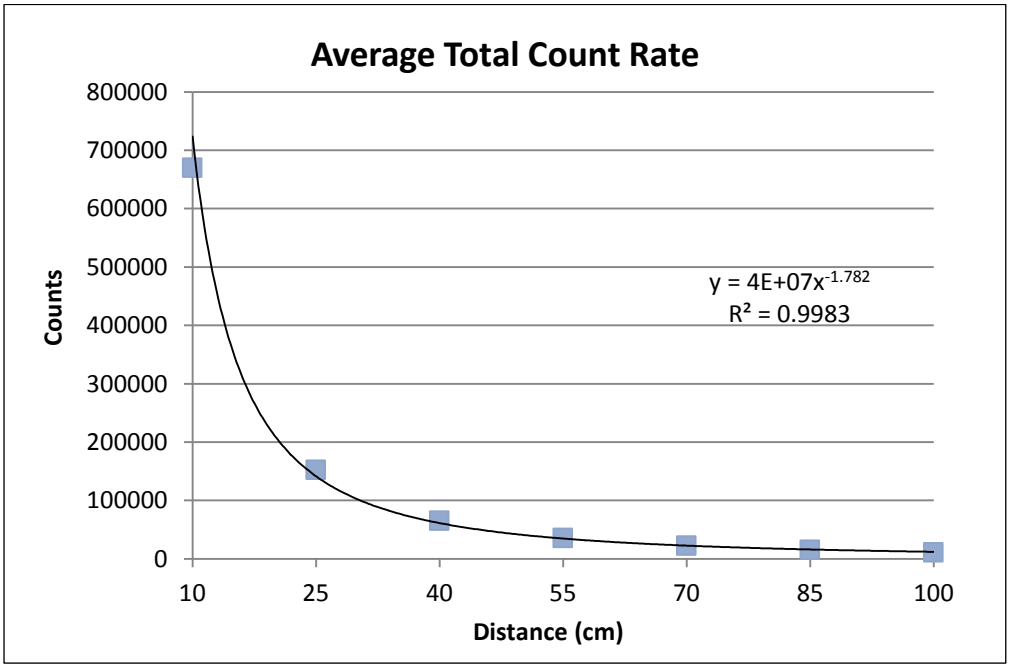

Figure 5.1 Average Total Count Rate for All 7 Data Points

5.2 Program Output

Next the FORTRAN program was utilized to calculate the total efficiency of the detector as a function of the distance between the source and detector. 10,000 trapezoids were used in the program for the area approximation of the area under the curve produced by the efficiency equation. The value for the attenuation coefficient was varied by a factor of ± 0.50e-5. The accepted value for the attenuation coefficient of air provided by NIST is $9.55\ x\ 10^{-5}$. The efficiency values calculated for each distance were written into a file in which was copied and pasted into an Excel spreadsheet for calculations.

Efficiency			
CM	$\mu_a = 9.55e-5$	$\mu_a = 1.05e-4$	$\mu_a = 9.05e-5$
10	0.020991011	0.020988965	0.020992102
25	0.004316112	0.004315088	0.004316648
40	0.001801856	0.001801168	0.001802215
55	0.000982336	0.000981823	0.000982606
70	0.000616803	0.000616393	0.000617019
85	0.000422758	0.000422416	0.000422938
100	0.000307592	0.000307300	0.000307746

Table 5.2 Efficiency for Varying Attenuation Coefficients

5.3 Final Results

Using the calculated efficiencies values, the average total count rates were divided by each of the respective efficiencies in Excel to obtain a value proportional to the total emission counts of Cs 137. For example, for the distance of 100 cm and the attenuation coefficient of 9.55e-5, the calculation was as follows:

$$\frac{11285.65\ counts}{0.000307592} = 36{,}690{,}311.90\ total\ emission$$

Total Emission = Total Count Rate / Efficiency			
CM	$\mu_a = 9.55e-5$	$\mu_a = 1.05e-4$	$\mu_a = 9.05e-5$
10	31922710.3	31925820.9	31921050.4
25	35303702.2	35312087.5	35299322.5
40	36367476.1	36381358.4	36360221.8
55	36482476.4	36501553.0	36472440.0
70	36345082.7	36369224.5	36332362.3
85	36617783.6	36647367.2	36602201.1
100	36690311.9	36725147.5	36671904.4

Table 5.3 Calculated Total Emission of Cs 137

Using the accepted attenuation coefficient of air was expected to produce values for total emission that were within a small range of each other. However, the calculated emission ranged from 31,900,000 to 36,700,000 – a difference of almost 5 million counts. The graph below provides a representation of the range of values obtained for calculated emission of the Cs 137 source.

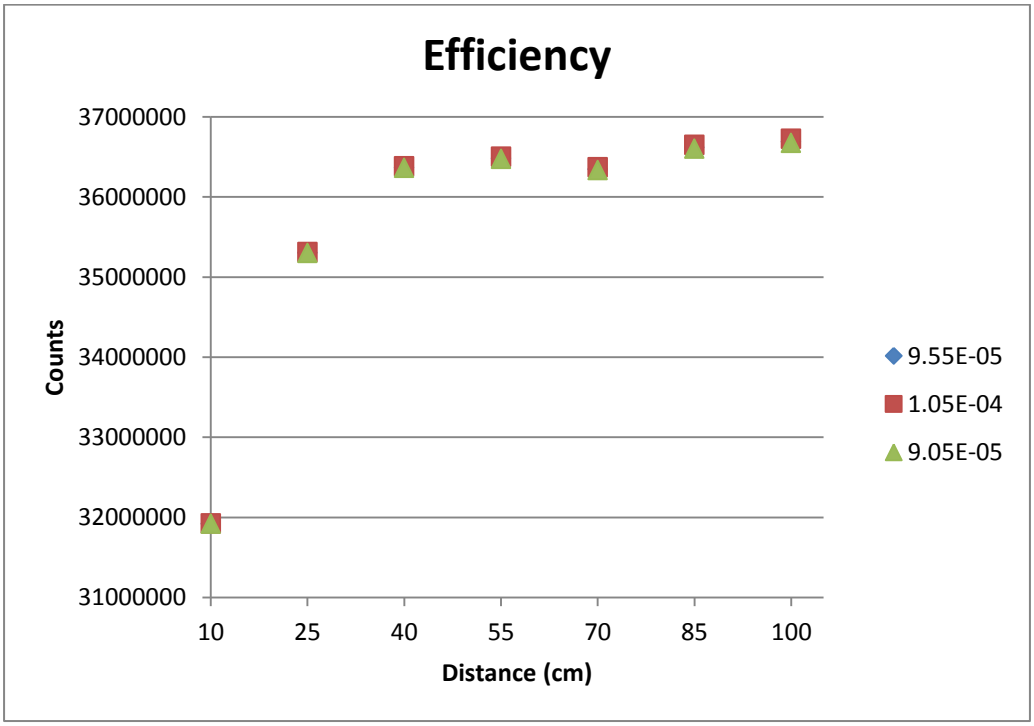

Figure 5.2 Calculated Total Emission of Cs 137 using all 7 Points

Looking at this data, it can be hypothesized that the data points at 10 cm and 25 cm may have been obtained at distances be too short to assume the source to be a point source. However, the other 5 data points suggest that using the efficiency is working well to correct for detection efficiency versus distance. So, only looking at the furthest 5 distances, the total emission graph looks close to a horizontal line (Figure 5.3).

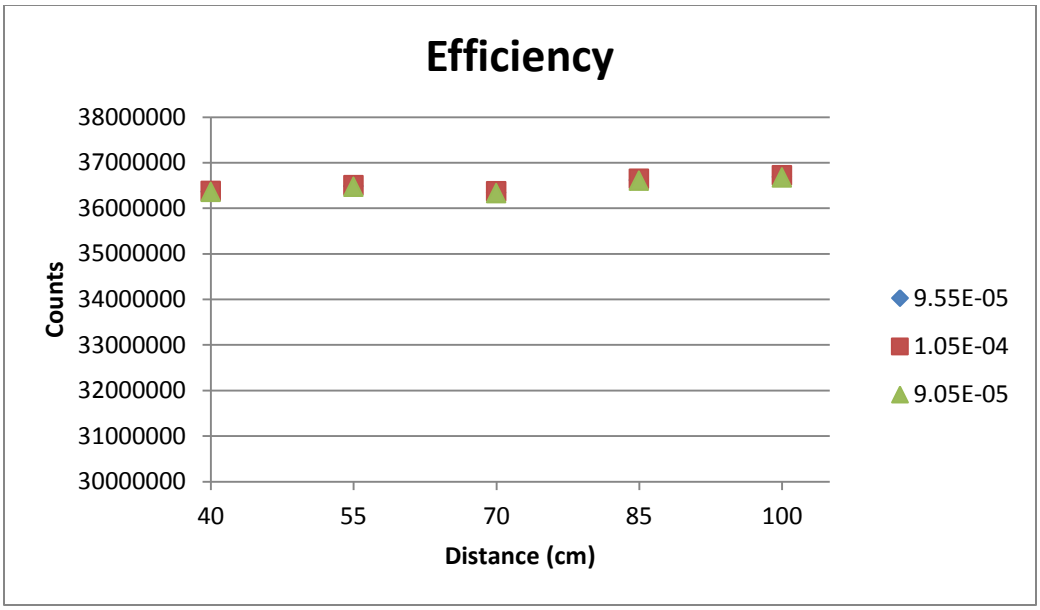

Figure 5.3 Calculated Total Emission using 5 Furthest Points

For the total average count rate graph in Figure 5.1, when the data was fit to a power trendline, the power of x was not 2, as would be expected for an inverse square law. Using the most distant 5 data points for the average total count rate graph produces a curve more similar to an inverse square law graph (Figure 5.4).

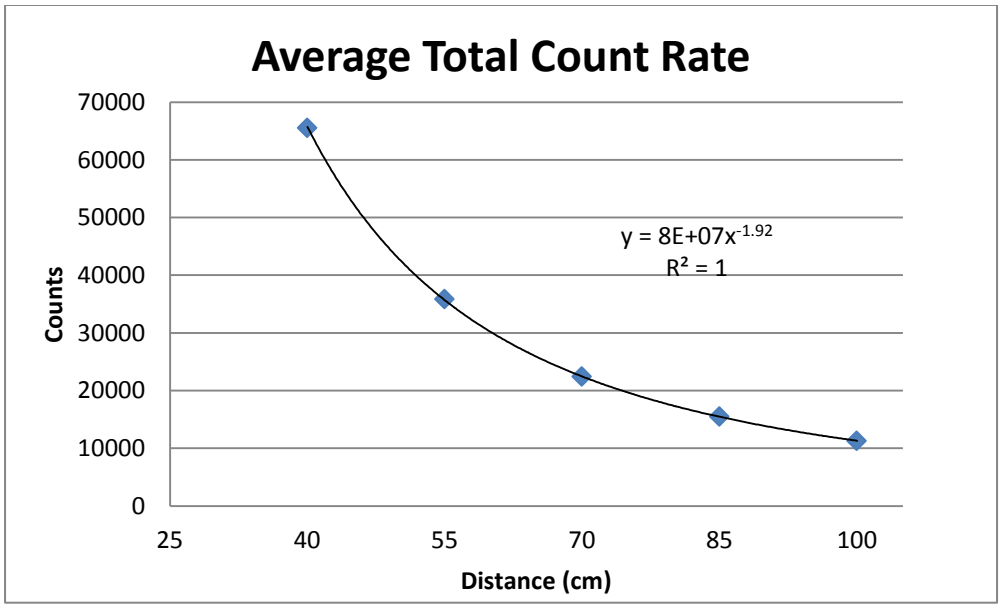

Figure 5.4 Average Total Count Rate for 5 Furthest Data Points

Here, the power of x is -1.92, which is much closer to -2 than -1.72 in Figure 3.1. So for any further calculations, only the furthest 5 data points will be used.

Also taken into consideration is the predicted count, which can be found using the predicted gamma rays emitted from the source, the FORTRAN code efficiency values, and a constant used to compensate for other efficiencies in the detection. The predicted count uses data from the FORTRAN code to predict the number of counts the detector should produce without using any experimental data.

$$\begin{gathered} Predicted\ Gamma\ Rays\ Emitted \\ = (Source\ Activity\ in\ Curies)\left(\frac{3.7x10^{10}decays}{(Ci * sec)}\right) \\ (Branching\ ratio)(Fraction\ of\ Cs-137\ remaining\ from\ half-life) \\ (Time\ detector\ ran) \end{gathered}$$

For example, for a 2400 second live-time, the number of gamma rays predicted is as follows:

$$\begin{gathered} Predicted\ Gamma\ Rays\ Emitted \\ = (1x10^{-6}C)\left(\frac{3.7x10^{10}decays}{Ci * sec}\right)\left(0.935\frac{gamma\ rays}{decay}\right)(0.95494)(2400\text{sec}) \\ = 79287117\ gamma\ rays \end{gathered}$$

The 0.935 gamma rays /decay value comes from the Cs-137 decay branching ratio as shown in Figure 1.4, and 0.95494was calculated using the information provided for the Cs-137 source.

$$\begin{gathered} Predicted\ Counts = \\ (Number\ of\ Gamma\ Rays\ Emitted) \\ (FORTRAN\ code\ efficiency\ \ values) \\ (other\ efficiency) \end{gathered}$$

Predicted Counts			
CM	9.55e-5	1.05e-4	9.05e-5
40	65768.867	65787.547	65758.920
55	35855.879	35861.002	35853.168
70	22513.690	22513.726	22513.674
85	15430.921	15428.731	15432.076
100	11227.304	11224.123	11229.000

Table 5.4 Calculated Predicted Counts

This other efficiency was found using the graph of the average total count rate (Figure 5.4). By plotting just the product of the predicted number of gamma rays emitted and the FORTRAN efficiency values, the graphs is as follows:

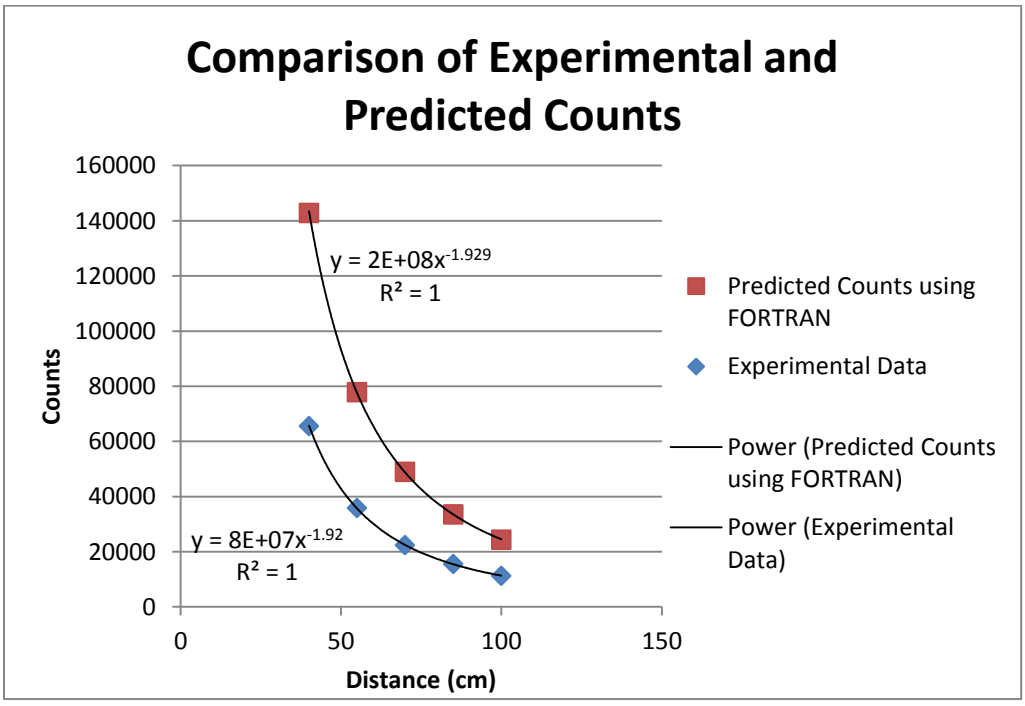

Figure 5.5 Comparison of Experimental Data and Predicted Counts (Not Using Constant – Efficiency Correction for Detector)

However, when a constant efficiency correction is factored into the predicted counts in addition to the distance-dependent corrections, a shift is produced so that the trend lines almost overlap (Figure 5.6). This constant is found by dividing the average

emission (determined by the experimental data) by the predicted emission (found using the FORTRAN code). Notice the power of x did not change, only the position of the curve was affected. This predicted data demonstrates remarkable agreement with the experimental data, especially considering that only a constant correction factor for other efficiencies was applied. The important information is contained in the shape of the curve (the exponent, *a*), not the magnitude of the curve.

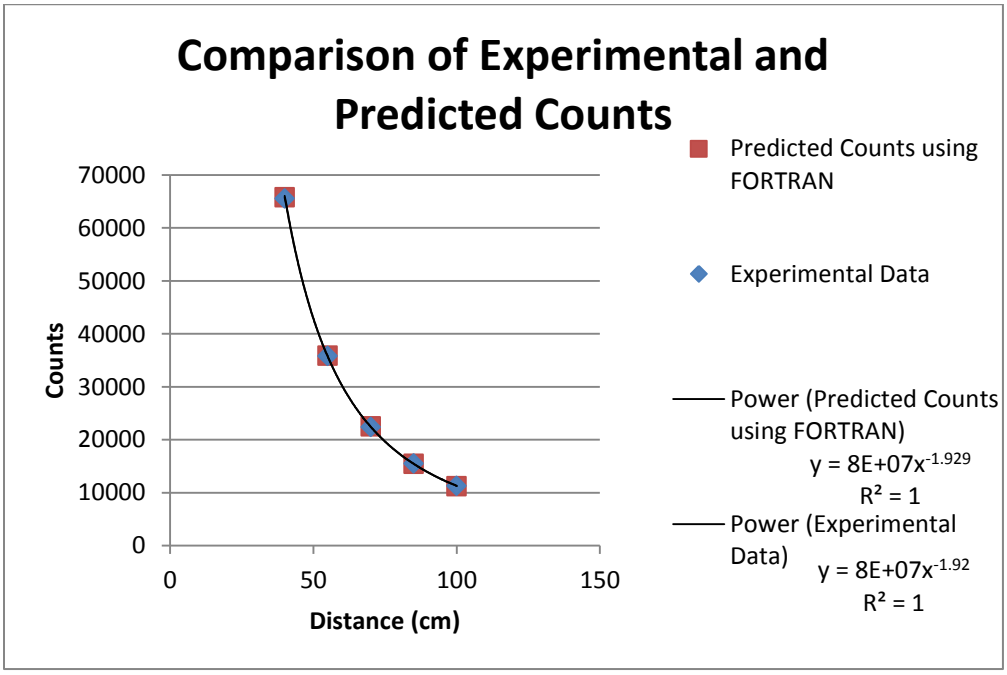

Figure 5.6 Comparison of Experimental Data and Predicted Counts (Using Constant – Efficiency for Detector)

Another model to predict the counts of the detector is the inverse square/attenuation model, which strictly uses calculation and no experimental data or programming. This model uses the calculated number of gamma rays emitted, the probability of a gamma ray striking the detector face ($A_d/4\pi r^2$ where A_d is the area of the detector face and r is distance), a correction for the atmospheric attenuation ($e^{-\mu r}$ where μ is the attenuation coefficient of air), and a constant detector efficiency (ε_o).

$$Number\ of\ Gamma\ Rays\ Counted = \frac{S_o A_d e^{-\mu r} \varepsilon_o}{4\pi r^2}$$

Using this inverse square/attenuation model, values for the number of gamma rays calculated were obtained for each distance.

$$S_o = 36500626.13$$
$$A_d = 45.6037\ cm^2$$
$$\mu = 9.55e^{-5}$$

CM	Number of Gamma Rays Counted
40	68076.50
55	35955.86
70	22165.46
85	15011.11
100	10830.01

Table 5.5 Inverse Square/Attenuation Model Calculated Counts

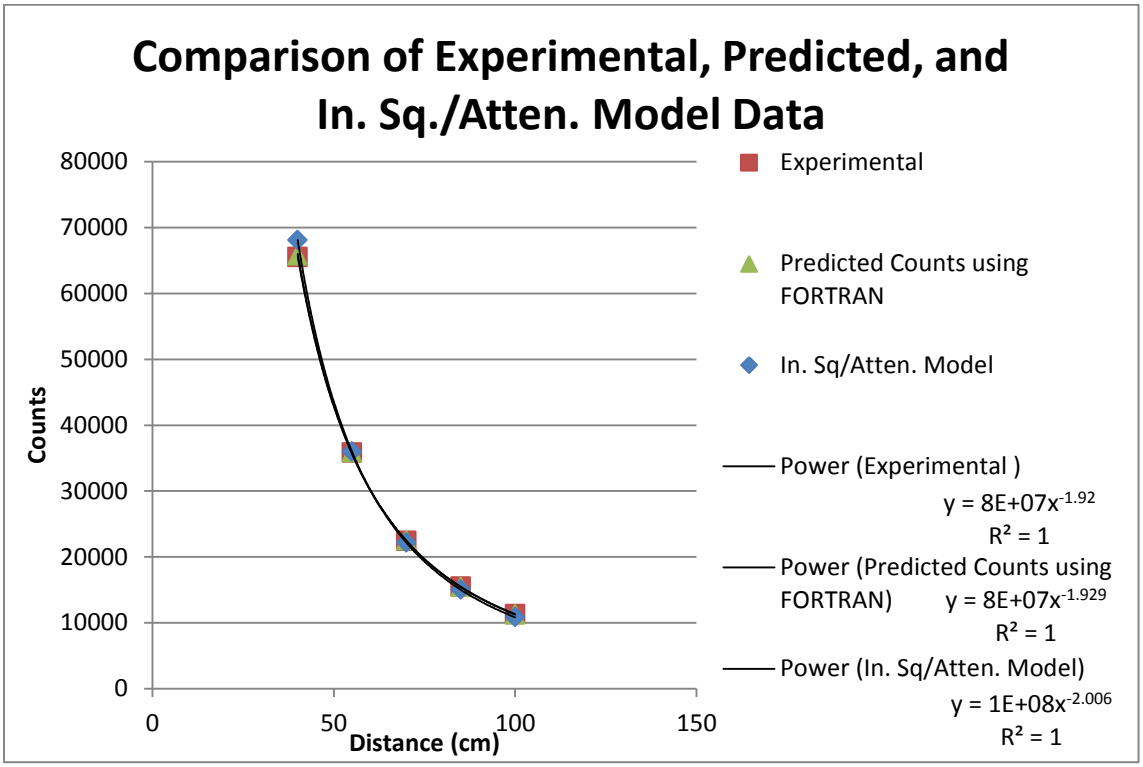

Figure 5.7 Comparison of Experimental Data, Predicted Counts, and Inverse Square/Attenuation Model Counts

Chapter 6 Conclusion

Ultimately, the results of our experiment and calculations should have allowed us to find a value for the attenuation coefficient of air that would create a single value for the total emission of Cs 137. We took into consideration the volume effect of the scintillator through the FORTRAN program and applied a correction – we called it efficiency. Those values of efficiency for each distance from the scintillator were applied to the experimental data as a percentage correction versus distance.

Once we calculated the total emission values, we found the first two data points (10 cm and 25 cm) to be inconsistent with the rest of the data. The first two data points gave a total emission within a range from 31,900,000 to 35,500,000, whereas the other 5 data points were all within a range from 36,300,000 to 36,800,000. This inconsistency is likely a result of our assumption that the source was a point source. Since the source was so close (within 25 cm) to the detector, we can no longer assume the source is a point source.

After excluding the first two data points, our data becomes much more consistent and gives better results. The experimental data (the average counts from the two data sets), when plotted and fit to a power function, gives an equation with $a = 1.92$. Plotting the predicted counts using the FORTRAN program gives us an equation with $a = 1.929$. The accuracy of this predicted data when compared to the experimental counts is extremely close and should not be dismissed. Notice both of these values for a are less than 2. When the inverse square/attenuation model counts were plotted, the value for a

was slightly larger than 2, which was to be expected for the inverse square law with attenuation added.

Our ability to plot these different predicted counts and the experimental data with values within about 3,000 counts of each other is significant. This is encouraging in our effort to find a method for measuring the attenuation coefficient of air using short distance radiation detection. Additional work will be required to determine how accurately the attenuation coefficient of air can be measured. However, at these short distances, the correction for detection efficiency versus distance is absolutely critical to successfully making such a measurement. The fact that the exponent of the power law fit is less than 2 for both the experimental data and the predicted data, which used the distance-dependent efficiency, is very relevant. The only way for an exponent less than 2 to occur is for effects other than attenuation and spherical spreading to be affecting the data. The primary effect at short distances is that gamma-rays incident on the detector at different angles can have very different detection efficiencies. These different efficiencies are due to the strong angle dependence of the gamma-ray path length in the NaI detector for short distances. The FORTRAN code approach seems to be very accurately correcting for this effect.

Literature Cited:

[1] American Cancer Society. Radiation Exposure and Cancer. 2010. <http://www.cancer.org/Cancer/CancerCauses/OtherCarcinogens/MedicalTreatments/radiation-exposure-and-cancer> October 2011.

[2] Environmental Protection Agency. "Radiation: Ionizing and Non-Ionizing". 2007. < http://www.epa.gov/radiation/understand/index.html> March 2013.

[3] Calvente, I., Fernandez, M.F., Olea, N., Nuñez, M.I., Villalba, J. "Exposure to electromagnetic fields (non-ionizing radiation) and its relationship with childhood leukemia: A systematic review." Science of The Total Environment. Volume 408, Issue 16. July 2010. Pages 3062-3069. <http://www.sciencedirect.com/science/article/pii/S0048969710003104> November 2011.

[4] Lei Li, Michael Story, Randy J Legerski. "Cellular responses to ionizing radiation damage." International Journal of Radiation Oncology*Biology*Physics. Volume 49, Issue 4. March 2001. Pages 1157-1162. <http://www.sciencedirect.com/science/article/pii/S0360301600015248> November 2011.

[5] Khan, F.M. The Physics of Radiation Therapy: Second Edition. Williams & Wilkins. 1994.

[6] Martensen, K., Snively, K. Rappel, Bowers, Parsons. "CT Dictionary." 2011. <http://wiki.uiowa.edu/display/881886/CT+Dictionary> November 2011.

[7] Idaho State University. “Gamma Radiation.” The Radiation Information Network. <http://www.physics.isu.edu/radinf/gamma.htm> February 2013.

[8] Hubbell, J.H.; Seltzer, S.M. Tables of X-Ray Mass Attenuation Coefficients and Mass Energy-Absorption Coefficients from 1 keV to 20 MeV for Elements Z = 1 to 92 and 48 Additional Substances of Dosimetric Interest. Ionizing Radiation Division, Physics Laboratory, NIST. 1996. <http://www.nist.gov/pml/data/xraycoef/index.cfm> September 2011

[9] Tsoulfanidis, N. Measurement and Detection of Radiation. McGraw-Hill, New York. 1983. March 2013.

[10] Ouseph, P.J. Introduction to Nuclear Radiation Detectors. Plenum Press, New York. 1975. March 2013.

[11] Lapp, R.E., Andrews, H.L. Nuclear Radiation Physics. Prentice-Hall, New Jersey. 1972. March 2013.

[12] Wang, W.H. “The Operational Characteristics of a Sodium Iodide Scintillation Counting System as a Single-Channel Analyzer.” Radiation Protection Management. Volume 20, No. 5. Radiation Safety Associates, Inc. 2003. April 2013.

[13] NDT Resource Center. “Radiographic Inspection – Formula Based on Newton’s Inverse Square Law.” <http://www.ndt-ed.org/GeneralResources/Formula/RTFormula/InverseSquare/InverseSquareLaw.htm> April 2013.